Electronic Supplementary Information

Improved Oxygen Evolution Activity of IrO_2 by *in situ* Engineering of Ultra-Small Ir Sphere Shell Utilizing Pulse Laser

Wenwu Zhong, Zhiping Lin, Shangshen Feng, Da Wang, Shijie Shen, Qinghua Zhang, Lin Gu, Zongpeng Wang* and Baizeng Fang**

Prof. W. W. Zhong, Dr. Z. P. Lin, Prof. S. S. Feng, Dr. S. J. Shen, Dr. Z. P. Wang
Department of Chemistry and Material Engineering
School of Advanced Study
Taizhou University
Taizhou, Zhejing, 318000, P. R. China
E-mail: zplin@tzc.edu.cn (Z. Lin); wangzp@tzc.edu.cn (Z. Wang)

Dr. D. Wang, Prof. Q. H. Zhang, Prof. L. Gu
Institution of Physics
Chinese Academy of Science
Beijing, 100190, China

Dr. Baizeng Fang
Department of Chemical & Biological Engineering
The University of British Columbia
2360 East Mall, Vancouver, B.C., V6T 1Z3, Canada
E-mail: bfang@chbe.ubc.ca

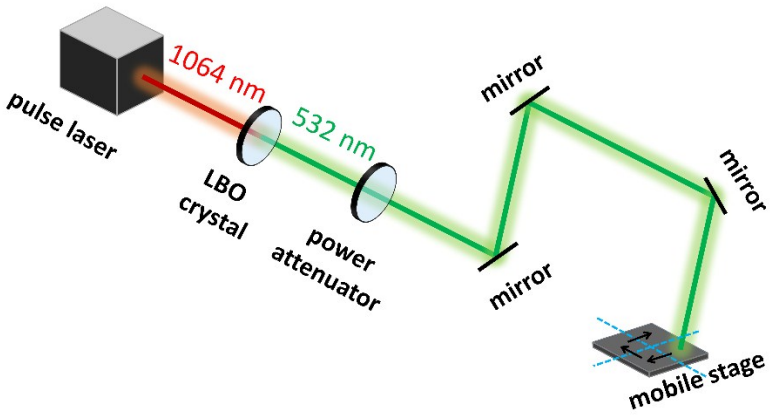

Figure S1. Illustration of the experimental setup. A LBO crystal is used to double the frequency illuminated from the laser in order to make the light line visible.

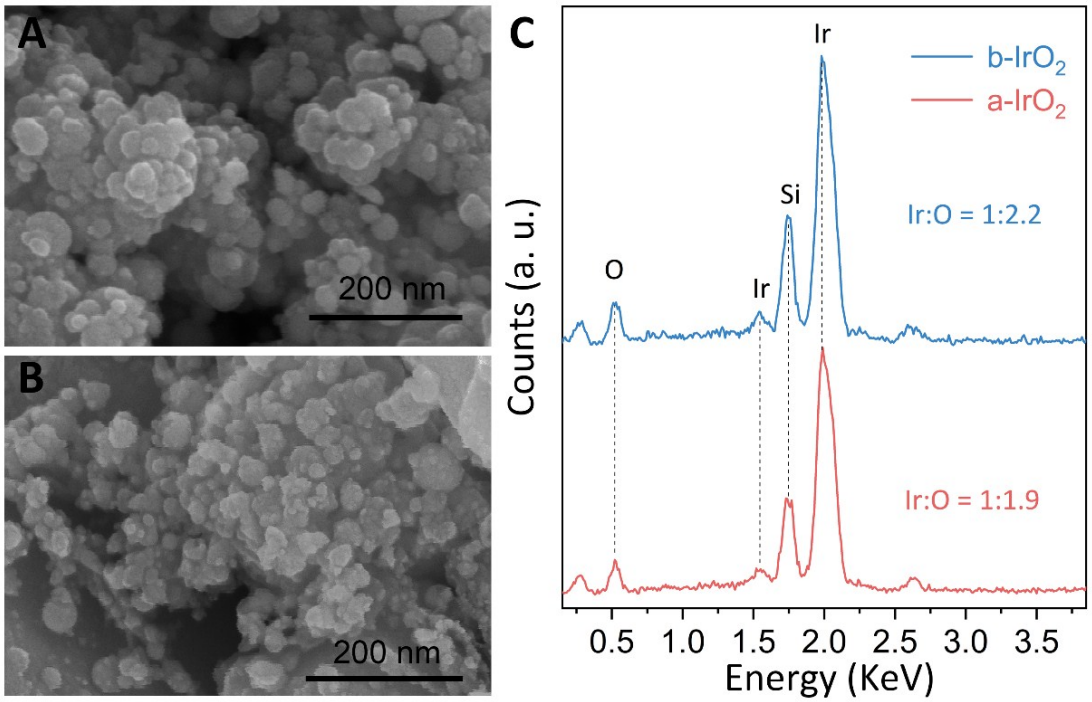

Figure S2. A, B) SEM images of the b-IrO_2 and a-IrO_2, respectively, and **C)** EDX analyses of the b-IrO_2 and a-IrO_2. The ratios shown in Figure S2C are atomic ratios.

Table S1. EDX elemental analysis for the IrO_2 before and after the laser modification.

Element	Atomic Ratio (%)	
	b-IrO_2	a-IrO_2
O	54.93	52.83
Si	20.15	19.08
Ir	24.92	28.09

Table S2. ICP analysis for the IrO_2 samples before and after the laser modification.

Element	Normalized content of Ir (%)	
	b-IrO_2	a-IrO_2
Ir	100	123

Notes: The content of Ir in the a-IrO_2 was normalized by the content of Ir in the b-IrO_2.

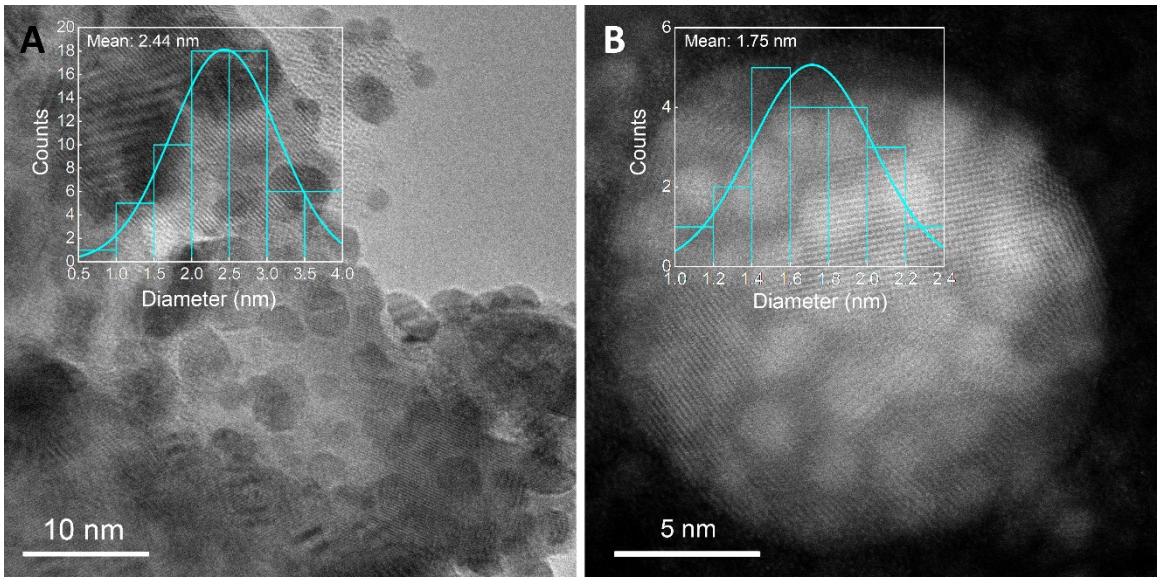

Figure S3. A) TEM image of the a-IrO_2, and **B)** HRTEM image of the a-IrO_2: Small Ir spheres (ca. 2 nm) are distributed on the surface of an IrO_2 sphere with a large size (over 20 nm). The insets in A and B are the statistics for the Ir sphere diameter.

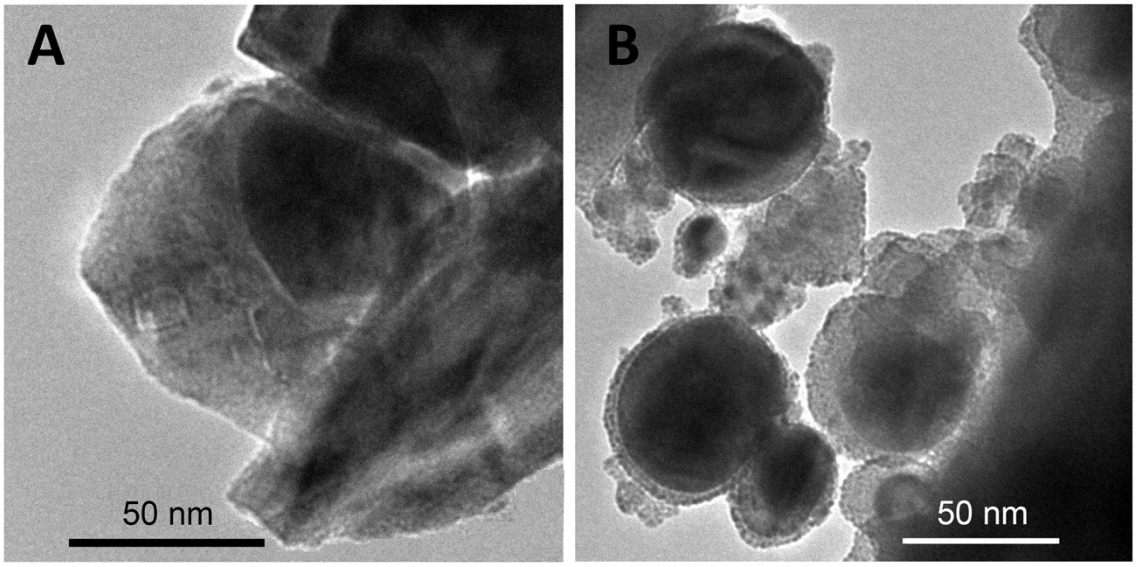

Figure S4. A) and **B**) TEM images of the b-IrO_2 and a-IrO_2, respectively.

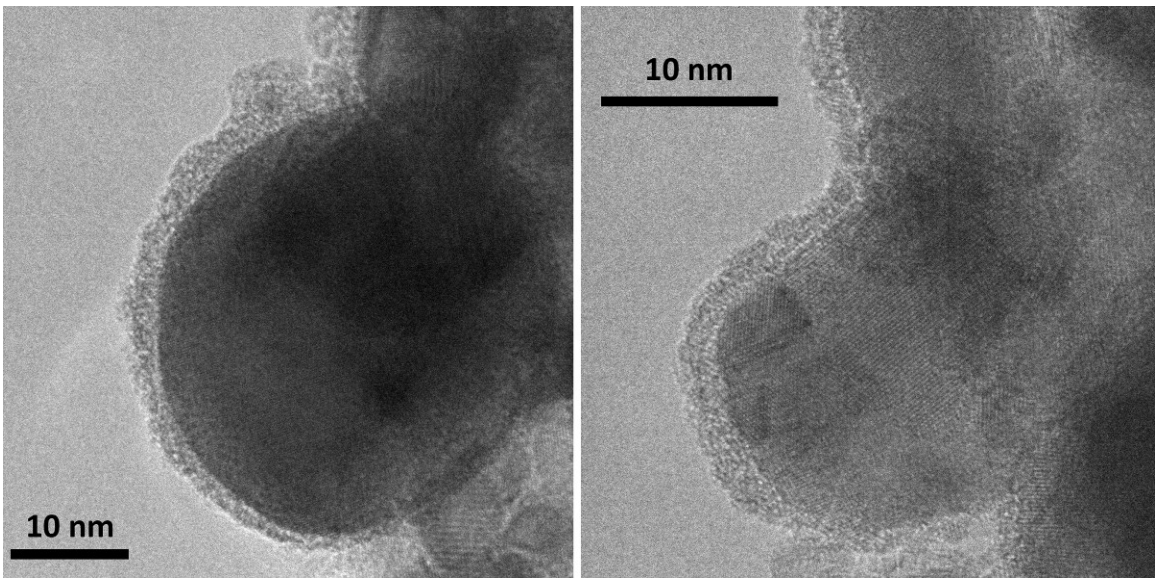

Figure S5. HRTEM images of the a-IrO_2.

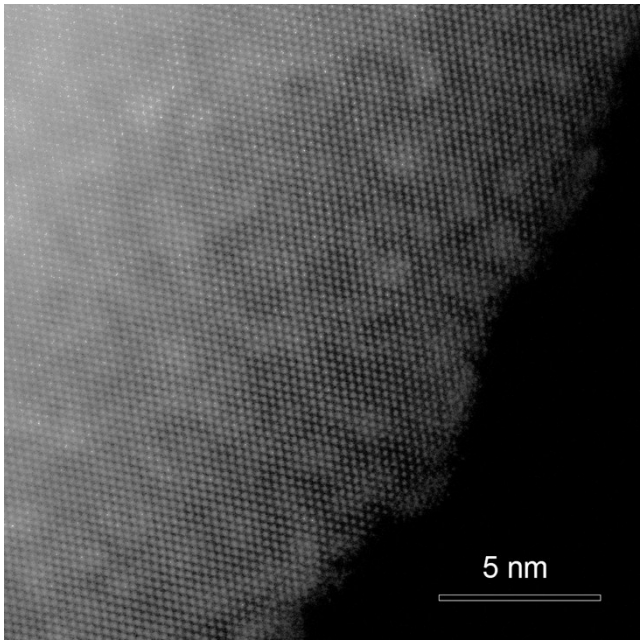

Figure S6. The enlarged TEM image of Figure 2C with reduced brightness.

Table S3. Details of the crystal structures of Ir and IrO_2 summarized from their PDF cards

	Crystal	**Space group**	***a* (Å)**	***c* (Å)**
Ir (JCPDS 46-1044)	cubic	Fm-3m(225)	3.840	-
IrO_2 (JCPDS 15-0870)	tetragonal	P42/mnm(136)	4.498	3.154

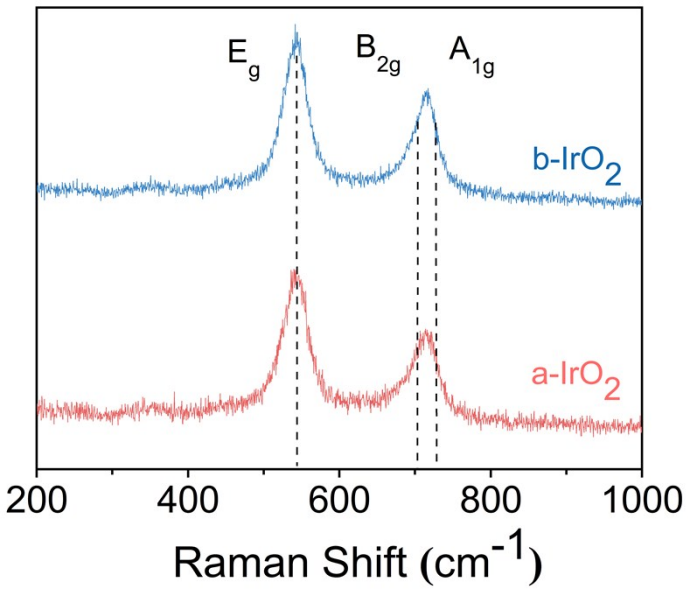

Figure S7. Raman spectra of the b-IrO_2 and a-IrO_2.

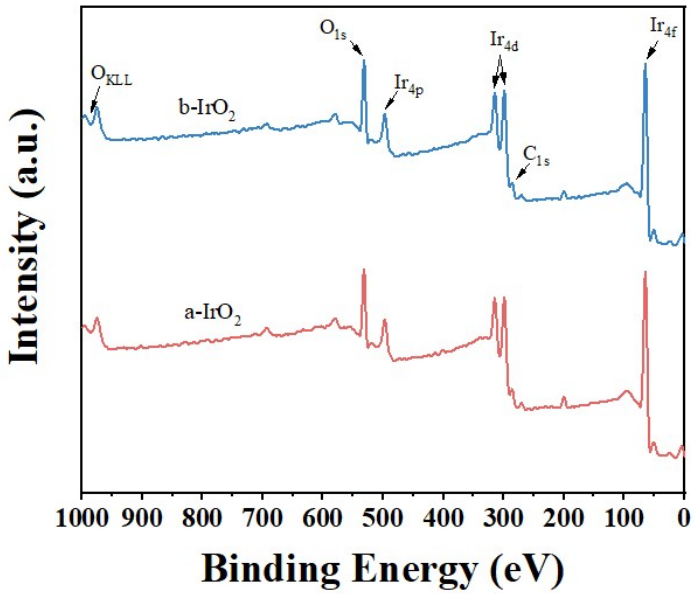

Figure S8. XPS survey spectra of the IrO_2 before and after the laser modification.

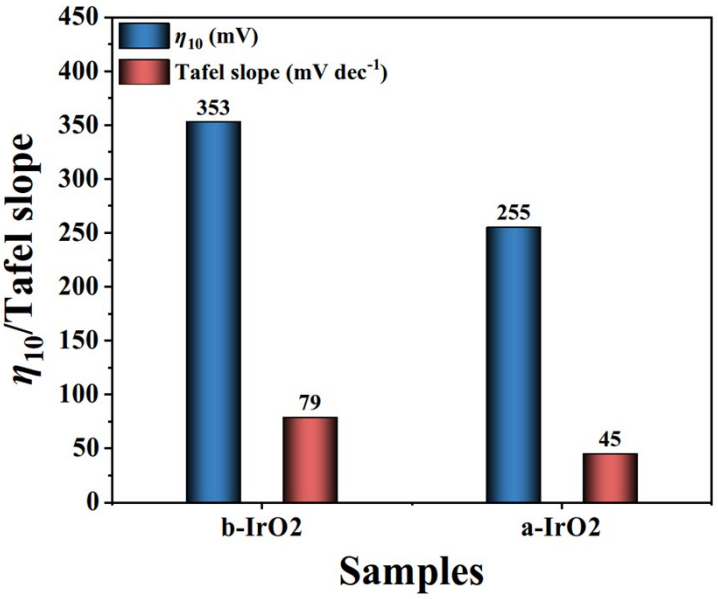

Figure S9. Bar chart for the summary of η_{10} values and Tafel slopes for the IrO_2 before and after the laser modification.

Table S4. Comparison of the OER performance of the a-IrO_2 and b-IrO_2 samples in alkaline solution with other representative OER catalysts reported in literature.

Catalyst	Electrolytes	Substrate	η_{10} (mV)	Tafel slope (mV dec^{-1})	Reference
RuO_2	0.5 M KOH	FTO	358	55	*ACS Nano*, 2015, **9**, 1977.
IrO_2	0.5 M KOH	FTO	411	91	
$CaCu_3Fe_4O_{12}$	0.1 M KOH	GCE	400	51	*Nat. Commun.*, 2015, **6**, 8249.
$CaFeO_3$	0.1 M KOH	GCE	390	47	
$SrFeO_3$	0.1 M KOH	GCE	410	63	
$LaFeO_3$	0.1 M KOH	GCE	500	77	*Chem. Mater.*, 2016, **28**, 1691.
$MnFe_2O_4$	0.1 M KOH	GCE	470	114	*Nanoscale*, 2015, **7**, 8920.
$CoFe_2O_4$	0.1 M KOH	GCE	370	82	
$NiFe_2O_4$	0.1 M KOH	GCE	440	98	
$CuFe_2O_4$	0.1 M KOH	GCE	410	94	
Co_3O_4	1 M KOH	Au	400	49	*Chem. Mater.*, 2012, **24**, 3567.

CoO_x-4h	1 M KOH	GCE	306	65	*Nano Energy*, 2018, **43**, 110.
Au@$CoFeO_x$	1 M KOH	GCE	328	58	*Nano Lett*., 2017, **17**, 6040.
CoO hexagrams	1 M KOH	GC	269	64.4	*Chem. Sci*., 2018, **9**, 6961.
$CoCr_2O_4$	1 M KOH	GCE	422	63.3	*Small*, 2016, **12**, 2866.
Fe–Ni nanoparticles	1 M NaOH	GCE	311	-	*ACS Catal*., 2016, **7**, 365.
Thin Ni–Fe hydroxide flm	1 M KOH	GCE	240	38.9	*Adv. Energy Mater*., 2017, **7**, 1770044.
$Co_{0.54}Fe_{0.46}OOH$	0.1 M KOH	GCE	390	47	*Sci. Rep*., 2017, **7**, 43590.
Ultrathin Co–Mn LDH	1 M KOH	GCE	324	43	*J. Am. Chem. Soc*., 2014, **136**, 16481.
Co–Fe LDH (1:0.35)	0.1 M KOH	GCE	350	49	*ChemSusChem*, 2017, **10**, 156.
Co–Cr LDH (2:1)	0.1 M KOH	GCE	340	81	*J. Mater. Chem. A*, 2016, **4**, 11292.
Exfoliated Ni–Fe nanosheets	1 M KOH	GCE	300	40	*Nat. Commun*., 2014, **5**, 4477.
Ni–Co 3D nanosheets	1 M NaOH	FTO	340	51	*Adv. Energy Mater*., 2015, **5**, 1500091.
Spindle-like $ZnCo_2O_4$	1 M KOH	GCE	389	60	*RSC Adv*., 2016, **6**, 92699.
$NiFe_2O_4$	1 M KOH	Carbon paper	360	40	*ACS Catal*., 2012, **2**, 1793.
$Co_{0.5}Mn_{0.5}WO_4$	0.1 M KOH	GCE	400	84	*ChemCatChem*, 2017, **9**, 1.
$Ni_{0.85}Fe_{0.15}O$	0.1 M KOH	GCE	328	42	*Adv. Sci.*, 2015, **2**, 1500199
$LiCo_{0.8}Fe_{0.2}O_2$	0.1 M KOH	GCE	340	50	*Adv. Mater*. 2015, **27**, 7150
$LiNi_{0.8}Al_{0.2}O_2$	0.1 M KOH	GCE	340	44	*Adv. Mater*., 2015, **27**, 6063.
α-$Co(OH)_2$	1 M KOH	GCE	380	67	*Dalton Trans*., 2017, **46**, 10545.
γ-CoOOH nanosheet	1 M KOH	GCE	300	38	*Angew. Chem. Int. Ed*., 2015, **54**, 8722
b-IrO_2	1 M KOH	GCE	**353**	**79.0**	**This study**
a-IrO_2	1 M KOH	GCE	**255**	**45.0**	

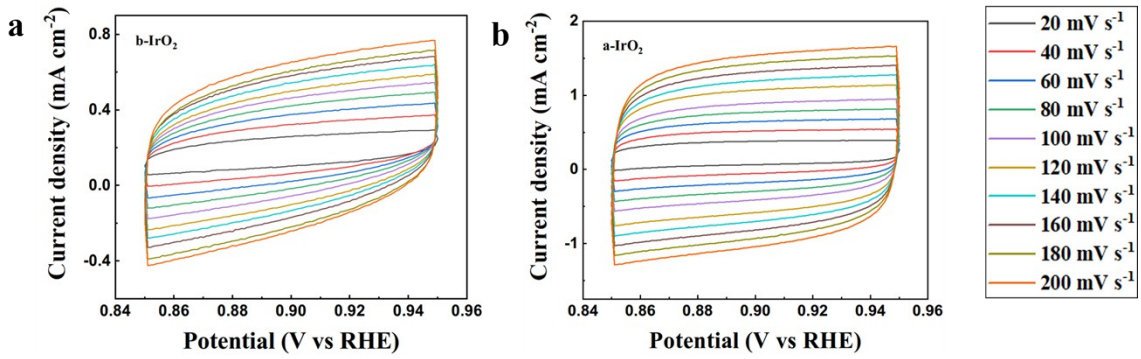

Figure S10. Cyclic voltammetry curves recorded in 1 M KOH at scan rates of 20, 40, 60, 80, 100, 120, 140, 160, 180 and 200 mV s^{-1} for the IrO_2 before (a) and after (b) the laser modification. The voltage window is 0.85–0.95 V vs. RHE.

Turnover frequency (TOF) is calculated by the equation: TOF = j*A/(4*F*n), where j is the electrode current density, A is the geometric area of the electrode, F is the Faraday constant of 96485 C mol^{-1}, n is the molar number of the active metal sites (Ir in this case) that were deposited on the electrode.[S1] The TOF of the a-IrO_2 is calculated to be 0.026 s^{-1} per active site at overpotential of 270 mV, whereas the TOF value of the b-IrO_2 is only 0.0018 s^{-1} per active site.

Electrochemically active surface area (ECSA): The ECSA of the catalyst can be calculated according to the equation: ECSA = C_{dl}/C_s, where C_{dl} is the double layer capacitance of the catalyst, C_s is the capacitance of the glass carbon electrode (C_s = 0.040 mF cm^{-2}).[S2] The LSV curves shown in Figure 4A are normalized by the ECSA, and shown in **Figure S11**.

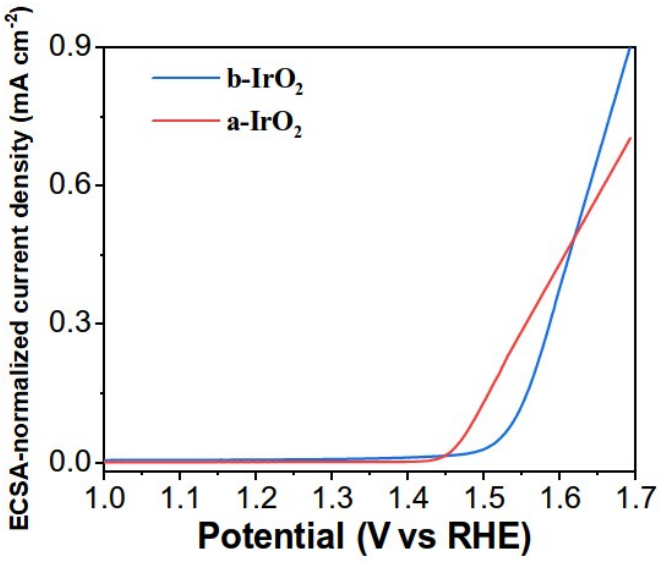

Figure S11. The LSV curves normalized by ECSA.

Table S5. Summary of the electrochemical data obtained for the IrO_2 before and after the laser modification.

Sample	OER Activity		C_{dl} (mF cm^{-2})	EIS	
	η @ j_{10} (mV)	Tafel Slope (mV dec^{-1})		R_s (Ω)	R_{ct} (Ω)
b-IrO_2	353	79	2.01	8.72	238.80
a-IrO_2	255	45	6.36	12.56	70.08

η: overpotential; **j_{10}:** current density of 10 mA cm^{-2}; **C_{dl}:** double layer capacitance; **R_s** and **R_{ct}:** electrolyte resistance and electron transfer resistance in the equivalent circuit.

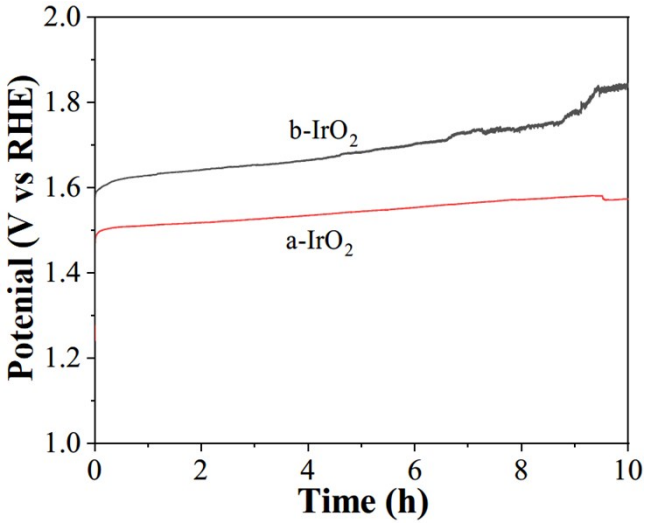

Figure S12. Time dependence of the overpotential recorded on the various IrO_2 materials.

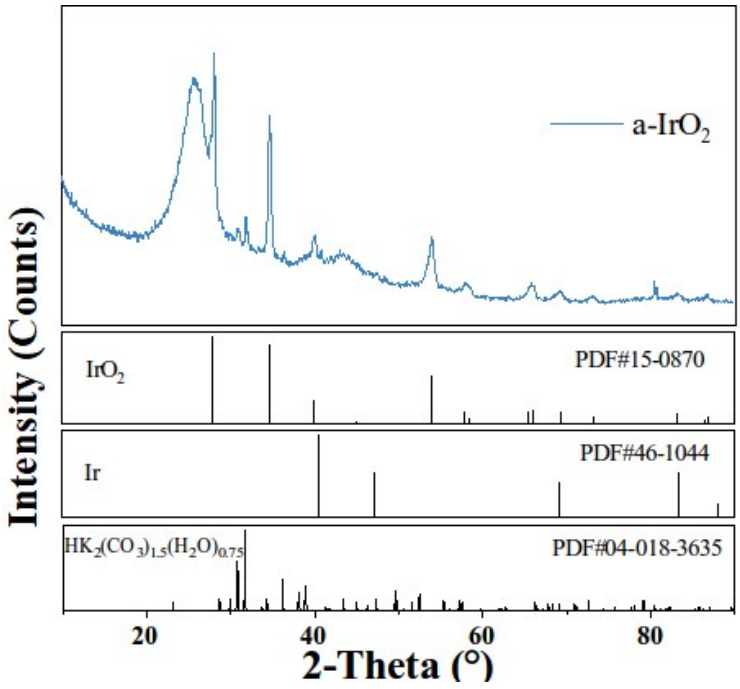

Figure S13. XRD patterns of the a-IrO_2 after the stability test. The impurity $HK_2(CO_3)_{1.5}(H_2O)_{0.75}$ may be generated by the reaction between the carbon cloth substrate and the electrolyte KOH.

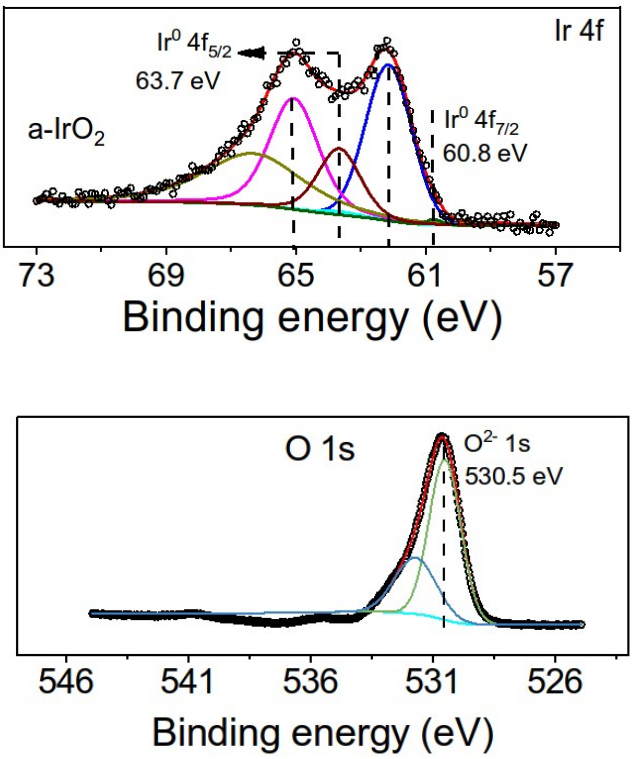

Figure S14. XPS spectra of the a-IrO_2 after the stability test.

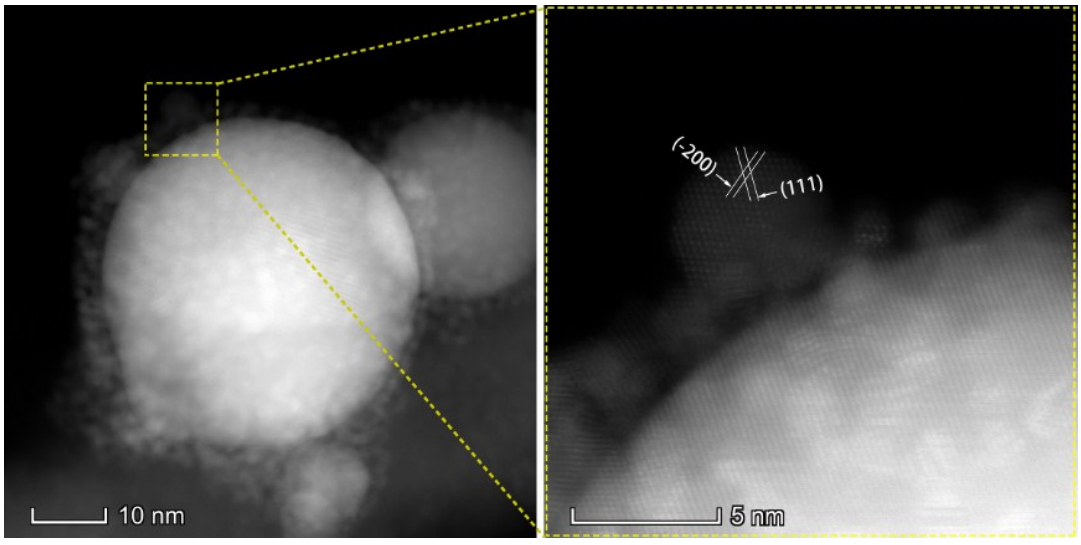

Figure S15. HRTEM images of the a-IrO_2 after the stability test.

References

S1. M. Gong, Y. Li, H. Wang, Y. Liang, J. Z. Wu, J. Zhou, J. Wang, T. Regier, F. Wei, and H. Dai, An advanced Ni–Fe layered double hydroxide electrocatalyst for water oxidation. *J. Am. Chem. Soc*., 2013, **135**, 8452-8455.

S2. C. C. McCrory, S. Jung, I. M. Ferrer, S. M. Chatman, J. C. Peters, and T. F. Jaramillo, Benchmarking hydrogen evolving reaction and oxygen evolving reaction electrocatalysts for solar water splitting devices. *J. Am. Chem. Soc*., 2015, **137**, 4347-4357.